IOP Publishing Journal of Physics B: Atomic, Molecular and Optical Physics
J. Phys. B: At. Mol. Opt. Phys. **47** (2014) 145003 (12pp) doi:10.1088/0953-4075/47/14/145003

Extreme ultraviolet spectra and analysis of $\Delta n = 0$ transitions in highly charged barium

J Reader, J D Gillaspy, D Osin and Yu Ralchenko

National Institute of Standards and Technology, Gaithersburg, MD 20899-8422, USA

E-mail: yuri.ralchenko@nist.gov

Received 14 March 2014, revised 3 June 2014
Accepted for publication 9 June 2014
Published 4 July 2014

Abstract

Extreme ultraviolet spectra of highly charged barium atoms were produced with an electron beam ion trap (EBIT) and recorded with a flat-field grazing-incidence spectrometer. The spectra were measured in the wavelength range 4 nm–24 nm with the beam energies varying from 700 eV to 30 000 eV. The line identifications were performed with collisional-radiative modeling of the EBIT plasma that provided good quantitative agreement between simulated and measured spectra. In the energy range 700 eV–1750 eV, fifty three $n = 4$–$n = 4$ transitions in Se-like (Ba^{22+}) to Cu-like (Ba^{27+}) ions were identified, with forty seven corresponding to new lines. Almost all lines are due to electric-dipole transitions. For the beam energies of 3945 eV–7530 eV, we identified eight new $n = 3$–$n = 3$ transitions in Ba^{42+} (Si-like), Ba^{43+} (Al-like), and Ba^{44+} (Mg-like). At the highest beam energy, 30 000 eV, three new $n = 2$–$n = 2$ transitions of Ba^{51+} (B-like), Ba^{52+} (Be-like), and Ba^{53+} (Li-like) were identified. The measured wavelengths are compared with recent *ab initio* theoretical calculations. An improved ionization energy for Ba^{26+} (Zn-like), IE = 937.2 ± 0.8 eV, was determined by comparing theoretical values with measurements along the Zn isoelectronic sequence.

Keywords: highly-charged ions, barium, extreme ultraviolet, EBIT

(Some figures may appear in colour only in the online journal)

1. Introduction

Barium is commonly used as a dopant in the electron gun cathode of electron beam ion traps (EBITs). As a result, atoms of barium are emitted from the cathode and migrate into the trap region. Once there, their spectra are excited along with spectra of injected elements. Indeed, spectra of Ba have been among the first investigated in nearly every EBIT. In our laboratory at the National Institute of Standards and Technology (NIST), we observed a magnetic-dipole transition in the ground configuration of Ba^{34+}(Ti-like) as one of the first investigations after completion of the machine in 1993. This line was seen in the visible/near ultraviolet region at 393.2 nm [1]. Spectra of Ba in the visible have also been reported from the Livermore EBIT [2, 3]. The x-ray spectra of Ba have been a subject of investigation on many EBITs. On the other hand, for the extreme ultraviolet (EUV) region of about 3 nm to 30 nm, there have been no other reports of Ba spectra from EBITs outside of our group. The present paper reports measurements and identifications of 64 spectral lines of Ba in the EUV. Almost all of them are newly observed.

These measurements were an outgrowth of observations performed to measure wavelengths of the D-lines of Na-like lanthanide ions [4]. At a beam energy of about 900 eV two extremely strong lines appeared in our spectra that clearly did not belong to an injected atom. We soon realized that these were the $4s^2\ {}^1S_0$–$4s4p\ {}^1P_1$ and $4s\ {}^2S_{1/2}$–$4p\ {}^2P_{3/2}$ resonance lines of Zn-like Ba^{26+} and Cu-like Ba^{27+}, respectively. Although these lines had been previously observed in laser-produced plasmas [5, 6], they had never been seen in an EBIT. We therefore decided to investigate the EUV spectra of Ba in our EBIT.

2. Experiment

The present measurements were carried out with the NIST EBIT. A review of its properties has been given by Gillaspy [7]. The experimental procedure for our measurements has

been described in detail in several recent papers [8, 9, 13]. For the present observations, we only used the Ba atoms emanating from the EBIT cathode. Electron beam energies were 700, 740, 790, 900, 830, 960, 1015, 1750, 3945, 5000, 5860, 7530, 8490, 8750, 9000, 10 000, 13 000, and 30 000 eV. The beam current varied between 15 mA and 150 mA.

A flat-field grazing-incidence spectrometer [10] was used to record EBIT spectra from 4.5 nm to 23.8 nm. A gold-coated variable-spaced grating used in the experiment had groove density of about 1200 lines per mm at the center of the grating. The spectra were recorded with a liquid nitrogen-cooled charge-coupled device (CCD) array having a matrix of 2048 pixels × 512 pixels. The full-width-at-half-maximum (FWHM) of our spectral lines was about 0.025 nm with a resolving power of approximately 500 at 12 nm. This FWHM represented about three pixel columns in the array.

At a given energy a complete spectrum consisted of five exposure frames of 60 s each, integrated to a whole. The spectra were corrected for spurious signals due to cosmic rays, and a background noise level of approximately 600 CCD analog-to-digital counts per pixel-column was subtracted from all spectra. Reference spectra consisted of lines of Fe^{19+}–Fe^{23+}, O^{4+}–O^{5+}, Ne^{4+}–Ne^{7+}, and Kr^{20+}–Kr^{33+}. A metal vapor vacuum arc ion source (MEVVA) [11] was used to inject Fe ions, while the gases were injected from a separate gas injection port. A pixel-to-wavelength conversion was produced with a fourth-degree polynomial fit of the reference spectral lines with a standard deviation of about 0.0008 nm. This represents the systematic uncertainty of our measurements. A Gaussian function was used to fit the measured line profiles. Statistical errors for strong lines were less than 0.001 nm. Our final wavelength for each line is the weighted average of the wavelengths measured at the various beam energies. The final uncertainties are the sum in quadrature of the statistical and systematic uncertainties.

The measured spectra for beam energies 740, 790, 830, and 1015 eV are given in figure 1. The vertically shifted curves show second-order lines, with wavelengths doubled and intensities reduced by a factor of three. A number of the identified lines are indicated in these spectra. In addition to the Ba lines, the measured spectra contain several impurity lines. The most prominent are the 16.44 nm line in Zn-like Xe^{24+} and the 22.115 nm line in Be-like Ar^{14+}. The presence of Xe is due to previously conducted experiments in which large amounts of Xe were injected into the EBIT and the ions extracted for surface-interaction studies. This left a persistent residue of Xe in the machine.

3. Collisional-radiative modeling and line identifications

In order to calculate the spectral line intensities in the measured range of wavelengths, we carried out collisional-radiative (CR) modeling of the Ba plasma. The modeling was performed with the CR code NOMAD [12] that has been extensively used for non-Maxwellian EBIT simulations [9, 13, 14]. The radiative and collisional data, such as level energies, radiative transition probabilities and electron-impact cross sections for excitation, de-excitation, ionization, and radiative recombination, were calculated with the Flexible Atomic Code (FAC) [15]. FAC uses the relativistic-model-potential method for determination of atomic wavefunctions and the relativistic distorted-wave approximation for calculation of electron-impact cross sections. The sizes of the atomic structure calculations varied with ion stage, depending on the complexity of electronic structure. For each beam energy they included up to seven thousand levels in 8–9 ions for a single calculation.

The calculated cross sections were fitted with simple formulas and collected in a database. Since the narrow Gaussian energy distribution of the EBIT beam did not overlap with the energies of dielectronic resonances, dielectronic capture was disregarded. Also, because the electron density in the trap is very low (on the order of 10^{12} cm^{-3}; this value was used in simulations), three-body recombination could be neglected.

Charge exchange (CX) with neutrals is an important recombination process affecting the ionization distribution in the trap. As was discussed in our previous papers (see, e.g., [16]), the CX rate is included as $R_{\rm CX} = N_0 \sigma_{\rm CX} v_r$, where N_0 is the density of background neutrals in the interaction region, $\sigma_{\rm CX}$ is the CX cross section, and v_r is the relative velocity between the highly-charged ions and the neutrals. We used a Classical Trajectory Monte–Carlo recommendation $\sigma_{\rm CX} \approx z \times 10^{-15}$ cm^{-2} [17] for the cross section of charge exchange with an ion of charge z. Since neither N_0 nor v_r are known experimentally, we used the previously developed collisional-radiative model for Xe ions [13] and the observed intensity ratios for the 16.44 nm line in the Zn-like Xe^{24+} and the 17.39 nm line in Cu-like Xe^{25+} to derive the product $N_0 v_r \approx 5 \times 10^{13}$ cm^{-2} s^{-1}. This value, which reasonably agrees with our previous estimates [16], was then used for the collisional-radiative modeling of the Ba spectra.

Figure 2 shows the observed spectrum of Ba at a nominal beam energy of 900 eV together with our simulated spectrum at 880 eV. This reduction of beam energy, the so-called space charge shift, is due to the presence of electrons in the trap region. These electrons repel incoming electrons in the beam and reduce the effective beam energy. As can be seen, agreement between the calculated and measured spectra is good. The inset in figure 2 shows the calculated ionization distribution of the EBIT plasma. As the ionization potential of Zn-like Ba^{26+} is about 937 eV (see below), the beam energy of about 880 eV to 900 eV is still too low to ionize it to the Cu-like ion.

Our identifications of the measured barium lines are given in table 1. The identifications were made by comparing the observed and calculated spectra. For individual lines, variation of the intensities with beam energy was used to establish charge stages. In several cases, variation of intensity with beam energy allowed us to obtain accurate wavelengths for lines belonging to different ion stages that are very close in wavelength. This analysis was particularly fruitful for identification of an otherwise-puzzling feature in the spectra at about 12.52 nm. This line appears strongly at beam

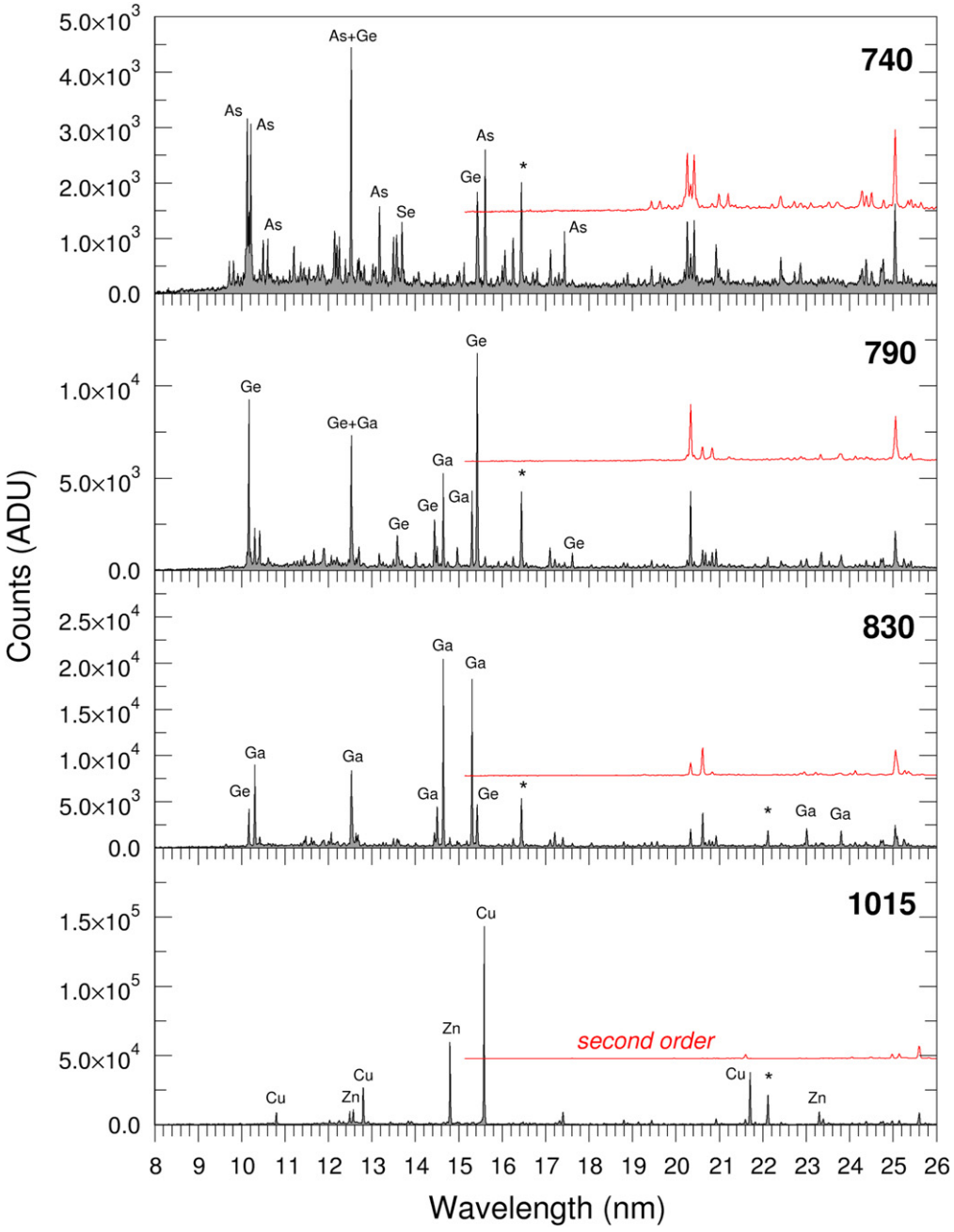

Figure 1. Measured spectra of Ba for beam energies 740, 790, 830, and 1015 eV in analog-to-digital units (ADU) of CCD. The second order lines (in red) are indicated by the vertically shifted curves. The nominal beam energies are shown in bold. The impurity lines from Xe^{25+} at 17.4 nm and Ar^{14+} at 22.1 nm are marked by asterisks.

energies of 700, 740, 790, and 830 eV, and is in fact the strongest of all the features in the spectrum at 740 eV. A very good spectral resolution and accurate modeling of the energy-dependent spectra allowed us to conclude that this feature was due to a coincidence of lines appearing at this wavelength from Ba^{23+}(As-like), Ba^{24+}(Ge-like) and Ba^{25+}(Ga-like). In Ba^{25+} it is actually a blend of two predicted transitions.

The transitions in table 1 are assigned according to the level designations from FAC, which are given in *jj*-coupling. The level numbers from FAC are also indicated. Here, 1 corresponds to the ground state, 2 corresponds to the first excited level, and so forth. In *jj*-designations, a minus sign indicates a *j*-value for an electron of $l-1/2$; a plus sign indicates a *j*-value of $l+1/2$.

4. Results

4.1. Beam energy 700 eV–1750 eV

In this range we observed $n=4$–$n=4$ transitions of N-shell ions Ba^{22+}(Se-like) to Ba^{27+}(Cu-like). As can be seen from the table, almost all of these lines are new. Of particular note are the new resonance lines of the Zn-like and Cu-like ions:

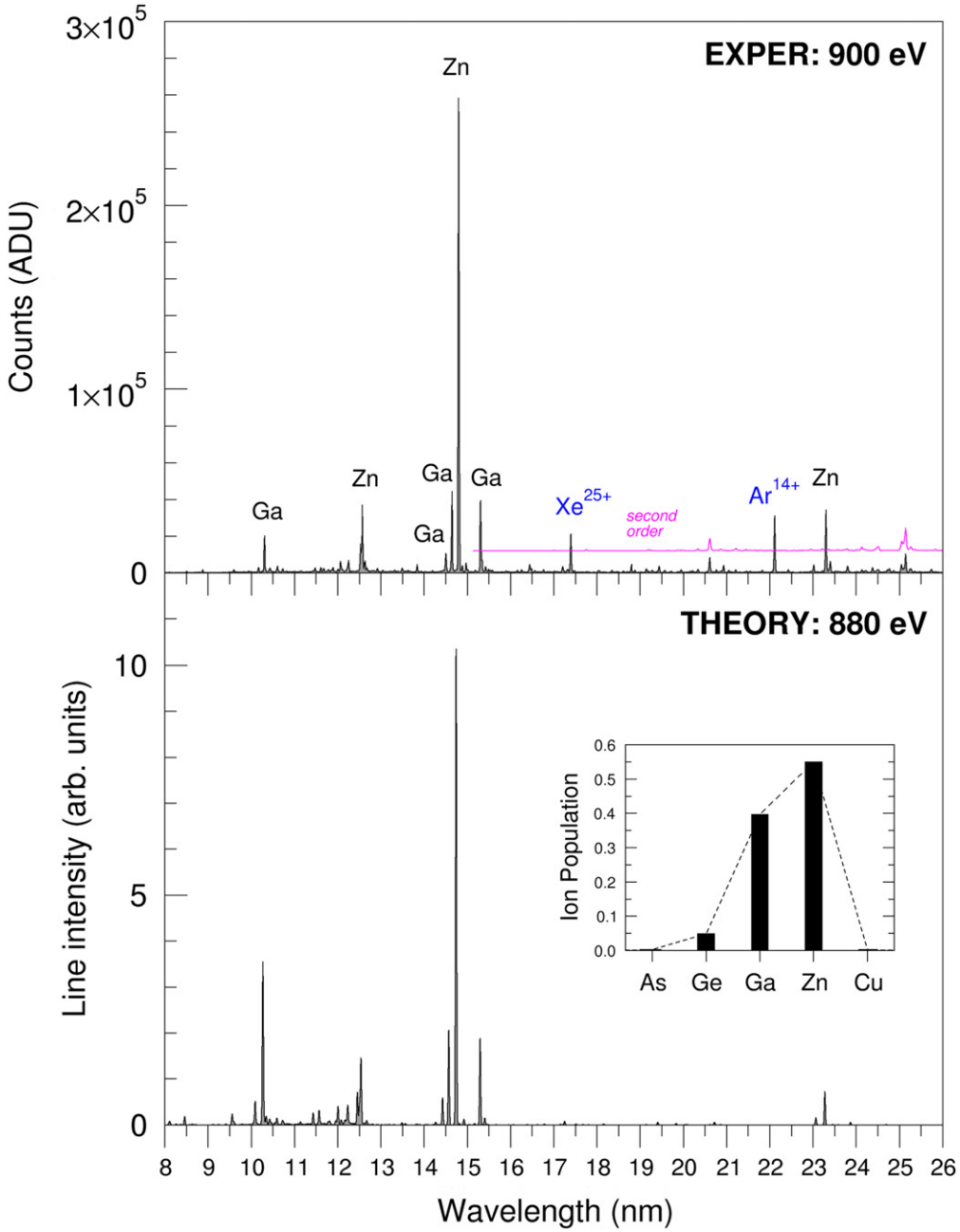

Figure 2. Observed spectrum of Ba at a beam energy of 900 eV (top) with our simulated spectrum calculated at 880 eV (bottom). The inset shows the calculated ionization distribution for Ba ions.

$(4s+^2)_0$–$(4s+, 4p-)_1$ for Ba^{26+} ($4s^2\ ^1S_0$–$4s4p\ ^3P_1$ in *LS* notation) and $(4s+)_{1/2}$–$(4p-)_{1/2}$ for Ba^{27+} ($4s\ ^2S_{1/2}$–$4p\ ^2P_{1/2}$ in *LS* notation).

4.2. Beam energy 3945 eV–7530 eV

In this energy range we observed $n = 3$–$n = 3$ transitions of M-shell ions Ba^{42+}(Si-like) to Ba^{44+}(Mg-like). The wavelengths and identifications of the measured lines, all of which are new, are given in table 1. Wavelengths for the lines of Na-like Ba are given in [4]. Our identification of the line at 12.6997 nm as the magnetic-dipole (M1) line of Al-like Ba is only tentative; it is shown with a question mark in table 1.

4.3. Beam energy 30 000 eV

At the highest energy, 30 keV, we observed spectral lines from B-like Ba^{51+}, Be-like Ba^{52+}, and Li-like Ba^{53+} (see figure 3). These are the first observed spectra for these ions in this spectral range. The Xe impurity lines are prominent here. The similarity of the L-shell spectra for Ba and Xe is clear in this spectrum.

4.4. Comparison with theory and with previous measurements

In table 2, we compare the present results with previous measurements and various theoretical values. The semi-empirical isoelectronic fits of [19, 20, 23, 24] clearly provide

Table 1. Experimental and theoretical wavelengths (nm) of highly charged ions of barium. New lines are noted as N.

Seq.	Stage	Wavelength (this work)	Uncert.		Wavelength (FAC)	Lower Config.	Lower Level	FAC Level	Upper Config.	Upper Level	FAC Level	Type
Se	22+	9.8174	0.0010	N	9.7409	$4s^24p^4$	$(4p+^2)_2$	1	$4s^24p^34d$	$((4p-,(4p+^2)_2)_{5/2},4d-)_3$	36	E1
Se	22+	10.0977	0.0010	N	10.0112	$4s^24p^4$	$(4p+^2)_2$	1	$4s^24p^34d$	$((4p-,(4p+^2)_2)_{5/2},4d+)_3$	33	E1
Se	22+	10.2425	0.0010	N	10.1590	$4s^24p^4$	$(4p+^2)_2$	1	$4s^24p^34d$	$((4p-,(4p+^2)_2)_{5/2},4d-)_2$	31	E1
Se	22+	10.5302	0.0012	N	10.4678	$4s^24p^4$	$(4p+^2)_2$	1	$4s^24p^34d$	$((4p-,(4p+^2)_2)_{3/2},4d+)_1$	28	E1
Se	22+	12.1919	0.0010	N	12.1372	$4s^24p^4$	$(4p+^2)_2$	1	$4s^24p^34d$	$(4p+,4d+)_3$	16	E1
Se	22+	12.7091	0.0010	N	12.6713	$4s^24p^4$	$(4p+^2)_2$	1	$4s^24p^34d$	$(4p+,4d+)_2$	14	E1
Se	22+	13.2868	0.0010	N	13.2460	$4s^24p^4$	$(4p+^2)_2$	1	$4s^24p^34d$	$(4p+,4d-)_1$	11	E1
Se	22+	13.5552	0.0010	N	13.5252	$4s^24p^4$	$(4p+^2)_2$	1	$4s^24p^34d$	$(4p+,4d-)_3$	10	E1
Se	22+	13.7319	0.0011	N	13.7000	$4s^24p^4$	$(4p+^2)_2$	1	$4s^24p^34d$	$(4p+,4d-)_2$	8	E1
Se	22+	15.5088	0.0010	N	15.4902	$4s^24p^4$	$(4p+^2)_2$	1	$4s4p^5$	$(4s+,(4p+^3)_{3/2})_1$	7	E1
Se	22+	16.7049	0.0011	N	16.7201	$4s^24p^4$	$(4p+^2)_2$	1	$4s4p^5$	$(4s+,(4p+^3)_{3/2})_2$	6	E1
As	23+	9.7176	0.0010	N	9.6238	$4s^24p^3$	$(4p+)_{3/2}$	1	$4s^24p^24d$	$((4p-,4p+)_2,4d-)_{5/2}$	29	E1
As	23+	9.8149[a]	0.0010	N	9.7580	$4s^24p^3$	$(4p+)_{3/2}$	1	$4s^24p^24d$	$((4p-,4p+)_1,4d+)_{3/2}$	28	E1
As	23+	10.1300[b]	0.0010	N	10.0423	$4s^24p^3$	$(4p+)_{3/2}$	1	$4s^24p^24d$	$((4p-,4p+)_2,4d-)_{1/2}$	27	E1
As	23+	10.1300[b]	0.0010	N	10.0443	$4s^24p^3$	$(4p+)_{3/2}$	1	$4s^24p^24d$	$((4p-,4p+)_2,4d-)_{3/2}$	26	E1
As	23+	10.2097	0.0010	N	10.1272	$4s^24p^3$	$(4p+)_{3/2}$	1	$4s^24p^24d$	$((4p-,4p+)_2,4d+)_{5/2}$	24	E1
As	23+	10.4949	0.0010	N	10.4234	$4s^24p^3$	$(4p+)_{3/2}$	1	$4s^24p^24d$	$((4p-,4p+)_1,4d+)_{3/2}$	22	E1
As	23+	10.6016	0.0010	N	10.5722	$4s^24p^3$	$(4p+)_{3/2}$	1	$4s^24p^24d$	$((4p-,4p+)_1,4d+)_{5/2}$	21	E1
As	23+	12.5229	0.0010	N	12.4852	$4s^24p^3$	$(4p+)_{3/2}$	1	$4s^24p^24d$	$(4d+)_{5/2}$	12	E1
As	23+	13.1766	0.0010	N	13.1355	$4s^24p^3$	$(4p+)_{3/2}$	1	$4s^24p^24d$	$(4d-)_{3/2}$	10	E1
As	23+	15.6099	0.0010	N	15.6067	$4s^24p^3$	$(4p+)_{3/2}$	1	$4s4p^4$	$(4s+,(4p+^2)_2)_{3/2}$	7	E1
As	23+	17.4362	0.0010	N	17.4909	$4s^24p^3$	$(4p+)_{3/2}$	1	$4s4p^4$	$(4s+,(4p+^2)_2)_{5/2}$	6	E1
Ge	24+	10.1687	0.0010	N	10.0897	$4s^24p^2$	$(4p-^2)_0$	1	$4s^24p4d$	$(4p-,4d-)_1$	17	E1
Ge	24+	10.4180	0.0010	N	10.3453	$4s^24p^2$	$(4p-,4p+)_2$	3	$4s^24p4d$	$(4p+,4d-)_3$	23	E1
Ge	24+	12.5272	0.0010	N	12.4972	$4s^24p^2$	$(4p-,4p+)_2$	3	$4s^24p4d$	$(4p-,4d+)_3$	16	E1
Ge	24+	13.5844	0.0011	N	13.5650	$4s^24p^2$	$(4p-,4p+)_2$	3	$4s^24p4d$	$(4p-,4d-)_2$	14	E1
Ge	24+	14.0102	0.0012	N	13.8297	$4s^24p^2$	$(4p-,4p+)_1$	2	$4s4p^3$	$((4s+,4p-)_1,(4p+^2)_2)_2$	13	E1
Ge	24+	14.4428	0.0010	N	14.2667	$4s^24p^2$	$(4p-,4p+)_2$	3	$4s4p^3$	$((4s+,4p-)_1,(4p+^2)_2)_2$	13	E1
Ge	24+	15.4254	0.0010	N	15.4037	$4s^24p^2$	$(4p-^2)_0$	1	$4s4p^3$	$(4s+,4p+)_1$	7	E1
Ge	24+	17.6117	0.0010	N	17.6749	$4s^24p^2$	$(4p-,4p+)_1$	2	$4s4p^3$	$((4s+,4p-)_0,(4p+^2)_2)_2$	8	E1
Ga	25+	10.3045	0.0010	N	10.2670	$4s^24p$	$(4p-)_{1/2}$	1	$4s^24d$	$(4d-)_{3/2}$	11	E1
Ga	25+	11.4770	0.0010	N	11.4328	$4s^24d$	$(4d-)_{3/2}$	11	$4s^24f$	$(4f-)_{5/2}$	42	E1
Ga	25+	11.6086	0.0010	N	11.5710	$4s^24p$	$(4p-)_{1/2}$	1	$4s4p^2$	$(4s+,(4p+^2)_2)_{3/2}$	10	E1
Ga	25+	12.0652	0.0010	N	12.0082	$4s^24p$	$(4p+)_{3/2}$	2	$4s^24d$	$(4d+)_{5/2}$	12	E1
Ga	25+	12.5264	0.0010	N	12.4546	$4s^24p$	$(4p+)_{3/2}$	2	$4s^24d$	$(4d-)_{3/2}$	11	E1
Ga	25+	12.5490[c]	0.0012	N	12.5057	$4s4p^2$	$((4s+,4p-)_1,4p+)_{3/2}$	6	$4s4p4d$	$((4s+,4p-)_1,4d+)_{5/2}$	24	E1
Ga	25+	14.5047	0.0010	N	14.4269	$4s^24p$	$(4p+)_{3/2}$	2	$4s4p^2$	$(4s+,(4p+^2)_2)_{3/2}$	10	E1
Ga	25+	14.6428	0.0010	N	14.5694	$4s^24p$	$(4p-)_{1/2}$	1	$4s4p^2$	$((4s+,4p-)_1,4p+)_{1/2}$	7	E1

Table 1. (Continued.)

Seq.	Stage	Wavelength (this work)	Uncert.		Wavelength (FAC)	Lower Config.	Lower Level	FAC Level	Upper Config.	Upper Level	FAC Level	Type
Ga	25+	15.3051	0.0010	N	15.2963	$4s^24p$	$(4p-)_{1/2}$	1	$4s4p^2$	$((4s+,4p-)_1,4p+)_{3/2}$	6	E1
Ga	25+	17.2064	0.0010	N	17.2498	$4s^24p$	$(4p+)_{3/2}$	2	$4s4p^2$	$(4s+,(4p+^2)_2)_{5/2}$	8	E1
Ga	25+	23.0121	0.0010	N	23.0659	$4s^24p$	$(4p-)_{1/2}$	1	$4s4p^2$	$(4s+)_{1/2}$	3	E1
Ga	25+	23.8007	0.0010	N	23.8650	$4s^24p$	$(4p+)_{3/2}$	2	$4s4p^2$	$((4s+,4p-)_1,4p+)_{5/2}$	5	E1
Zn	26+	9.5949	0.0010	N	9.5565	4s4p	$(4s+,4p-)_1$	3	4s4d	$(4s+,4d+)_2$	14	E1
Zn	26+	10.4346	0.0010	N	10.4196	4s4p	$(4s+,4p-)_0$	2	4s4d	$(4s+,4d-)_1$	11	E1
Zn	26+	12.2523	0.0010	N	12.2350	4s4d	$(4s+,4d+)_2$	14	4s4f	$(4s+,4f+)_3$	30	E1
Zn	26+	12.5704	0.0010	N	12.5381	4s4p	$(4s+,4p+)_1$	5	4s4d	$(4s+,4d+)_2$	14	E1
Zn	26+	14.7993	0.0010		14.7382	$4s^2$	$(4s+^2)_0$	1	4s4p	$(4s+,4p+)_1$	5	E1
Zn	26+	23.3015	0.0010	N	23.2735	$4s^2$	$(4s+^2)_0$	1	4s4p	$(4s+,4p-)_1$	3	E1
Cu	27+	10.8001	0.0010		10.7927	4p	$(4p-)_{1/2}$	2	4d	$(4d-)_{3/2}$	4	E1
Cu	27+	12.4879	0.0010		12.5916	4d	$(4d+)_{5/2}$	5	4f	$(4f+)_{7/2}$	7	E1
Cu	27+	12.8007	0.0010		12.7984	4p	$(4p+)_{3/2}$	2	4d	$(4d+)_{5/2}$	5	E1
Cu	27+	15.5827	0.0010		15.5415	4s	$(4s+)_{1/2}$	1	4p	$(4p+)_{3/2}$	3	E1
Cu	27+	21.7055	0.0010	N	21.5791	4s	$(4s+)_{1/2}$	1	4p	$(4p-)_{1/2}$	2	E1
Si	42+	4.5788	0.0010	N	4.5627	$3p^2$	$(3p-^2)_0$	1	3p3d	$(3p-,3d-)_1$	10	E1
Al	43+	4.7610	0.0010	N	4.7490	$3s^23p$	$(3p-)_{1/2}$	1	$3s^23d$	$(3d-)_{3/2}$	8	E1
Al	43+	5.5725	0.0010	N	5.5529	$3s^23p$	$(3p-)_{1/2}$	1	$3s3p^2$	$((3s+,3p-)_1,3p+)_{1/2}$	7	E1
Al	43+	5.7818	0.0010	N	5.7749	$3s^23p$	$(3p-)_{1/2}$	1	$3s3p^2$	$((3s+,3p-)_1,3p+)_{3/2}$	6	E1
Al	43+	11.5421	0.0010	N	11.5248	$3s^23p$	$(3p-)_{1/2}$	1	$3s3p^2$	$(3s+)_{1/2}$	3	E1
Al	43+	12.6697?	0.0010	N	12.6743	$3s^23p$	$(3p-)_{1/2}$	1	$3s^23p$	$(3p+)_{3/2}$	2	M1
Mg	44+	5.6815	0.0010	N	5.6603	$3s^2$	$^1S_0$	1	3s3p	$(3s+,3p+)_1$	5	E1
Mg	44+	12.3045	0.0012	N	12.2890	$3s^2$	$^1S_0$	1	3s3p	$(3s+,3p-)_1$	3	E1
B	51+	7.1809	0.0013	N	7.1524	$2s^22p$	$(2p-)_{1/2}$	1	$2s2p^2$	$(2s+)_{1/2}$	2	E1
Be	52+	9.2468	0.0012	N	9.2109	$2s^2$	$^1S_0$	1	2s2p	$(2s+,2p-)_1$	3	E1
Li	53+	9.8313	0.0010	N	9.7899	2s	$(2s+)_{1/2}$	1	2p	$(2p-)_{1/2}$	2	E1

[a] Blend with close line of Se-like Ba.
[b] Blend of two indicated transitions.
[c] Shoulder on long wavelength side of stronger Ga-like transition.

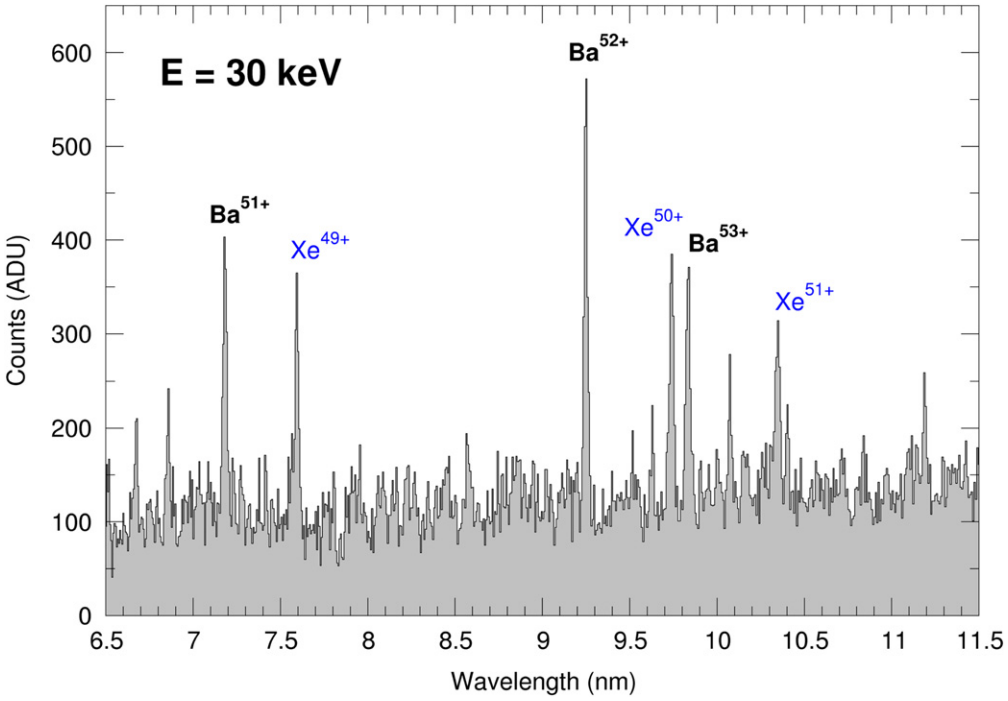

Figure 3. Observed spectrum of Ba at 30 keV.

very reliable results for Ba ions. The theoretical results for the M- and N-shell ions are relatively old and in some cases disagree with the measured wavelengths by as much as 1%. For the simpler L-shell B-, Be-, and Li-like ions of Ba, the recent advanced calculations with account of quantum electrodynamic effects [26, 28, 30] are in excellent agreement with our measurements, better than 0.03%. We hope that these data will stimulate new theoretical work.

4.5. Energy levels

In table 3, we give the energy levels of the Ba ions as determined by the present measurements. Several levels can only be determined with the aid of calculated values for the lower level of a transition. Since the lower level is not known experimentally in these cases, the energies are given with a '+*x*'. The level values for Cu-like Ba^{27+} are in reasonable agreement with those given in [6]; however, the present values have lower uncertainties than those in [6].

5. Ionization energies

Our analysis of the measured Ba spectra is based in part on the knowledge of ionization potentials of the ions under study. Ionization energies for Ba in all stages of ionization are given in the NIST Atomic Spectra Database (ASD) [32]. Most of these energies are taken from the relativistic Dirac–Fock calculations of Rodrigues *et al* [33]. This is true for all the ions of Ba in the present study. The one exception is Ba^{27+}(Cu-like), where a value of 976.62(11) eV was given by Reader *et al* [6]. The uncertainty that has been assigned to all of the calculated energies in ASD is 4 or 5 eV. It is possible to determine an improved value for the ionization energy of Ba^{26+}(Zn-like) by using the Rodrigues values in connection with experimental values for the Zn isoelectronic sequence.

In table 4 we give the total binding energies for selected Zn- and Cu-like ions calculated by Rodrigues *et al* [33]. The calculated ionization energy is formed as the difference of the values for the two ions. This table also presents the observed ionization energies for these ions taken from ASD. (The values for Se^{4+} and Kr^{6+} are semi-empirical, but are given with uncertainties, and for the present purpose we treat them as observed. The experimental value for Br^{5+} is taken from Riyaz *et al* [34].) The differences are plotted as filled circles in figure 4. The solid line is a weighted linear fit to these points. As can be seen, the observed values are higher than the theoretical values by a nearly constant 2–3 eV throughout the sequence.

In order to quantitatively evaluate this difference, and use it to apply a correction and overall uncertainty to the ionization energies calculated by Rodrigues *et al* [33], we assign a constant but unknown uncertainty to the calculated energies and then determine its value by requiring that the reduced chi square of the fit discussed in the previous paragraph be equal to 1. This constant of 0.52 eV is then added in quadrature to the experimental uncertainty to produce the total uncertainties in the points plotted in figure 4. The interpolated correction for Zn-like Ba is 2.55(60) eV (shown as a blue square in figure 4). The uncertainty of this correction is taken from the 68% confidence interval, plotted as dotted lines. Because this uncertainty is approximately one-half of the last significant digit tabulated by Rodrigues *et al* [33], we avoid the loss of a half-digit by applying the above correction not to the individual values in the tables, but to the value obtained by a three-parameter quadratic smoothing the calculated ionization

Table 2. Present wavelengths compared with other values. Notations: DHF—Dirac–Hartree–Fock, MCDF—multiconfiguration Dirac–Fock.

Stage	Seq.	Wavelength (nm)	Uncertainty (nm)	Method	Reference
26+	Zn	14.7993	0.0010	Present work	
		14.7972	0.0010	Laser-produced plasma	[18]
		14.7076		Theory—DHF	[19]
		14.7985		Semi-empirical; isoelectronic fit	[19]
26+	Zn	23.3015	0.0010	Present work	
		23.4284		Theory—DHF	[19]
		23.3015		Semi-empirical; isoelectronic fit	[19]
27+	Cu	10.8001	0.0010	Present work	
		10.8001	0.0015	Laser-produced plasma	[6]
		10.8037		Theory—DHF; Grant code	[20]
		10.8007		Semi-empirical; isoelectronic fit	[20]
27+	Cu	12.4879	0.0010	Present work	
		12.4876	0.0015	Laser-produced plasma	[6]
		12.4999		Theory—DHF; Grant code	[20]
		12.4900		Semi-empirical; isoelectronic fit	[20]
27+	Cu	12.8007	0.0010	Present work	
		12.7984	0.0015	Laser-produced plasma	[6]
		12.7944		Theory—DHF; Grant code	[20]
		12.7997		Semi-empirical; isoelectronic fit	[20]
27+	Cu	15.5827	0.0010	Present work	
		15.5770	0.0015	Laser-produced plasma	[6]
		15.5764		Theory—DHF; Grant code	[20]
		15.5808		Semi-empirical; isoelectronic fit	[20]
		15.5827		Theory—DHF; Desclaux code	[21]
		15.5813		Semi-empirical; isoelectronic fit	[21]
27+	Cu	21.7055	0.0010	Present work	
		21.6524		Theory—DHF; Grant code	[20]
		21.7063		Semi-empirical; isoelectronic fit	[20]
		21.7101		Theory—DHF; Desclaux code	[21]
		21.7053		Semi-empirical; isoelectronic fit	[21]
43+	Al	4.7610	0.0010	Present work	
		4.740 93		Theory—MCDF	[22]
43+	Al	5.5725	0.0010	Present work	
		5.528 65		Theory—MCDF	[22]
43+	Al	5.7818	0.0010	Present work	
		5.751 95		Theory—MCDF	[22]
43+	Al	11.5421	0.0010	Present work	
		11.423 87		Theory—MCDF	[22]
43+	Al	12.6697	0.0010	Present work	
		12.703 81		Theory—MCDF	[22]
44+	Mg	5.6815	0.0010	Present work	
		5.6770		Semi-empirical; isoelectronic fit	[23]
44+	Mg	12.3045	0.0012	Present work	
		12.299		Semi-empirical; isoelectronic fit	[23]
		12.2672		Theory—DHF; Grant code	[24]
		12.2983		Semi-empirical; isoelectronic fit	[24]
		12.302		Theory—Model Potential	[25]
51+	B	7.1809	0.0013	Present work	
		7.1773		Theory—DHF[a]	[26]
		7.1815		Theory—DHF[b]	[26]
		7.1654		Theory—Rel. DF	[27]
52+	Be	9.2468	0.0012	Present work	
		9.2486		Theory—DHF	[28]
		9.1946		Theory—Rel. DF	[29]
53+	Li	9.8313	0.0010	Present work	
		9.8346		Theory—DHF	[30]
		9.8332		Theory—DHF; Desclaux code	[31]
		9.8331		Semi-empirical; isoelectronic fit	[31]

[a] QED corrections estimated from hydrogenic self-energy
[b] QED corrections from screened model

Table 3. Energy levels of Ba ions from present measurements.

Seq.	Stage	Config.	Level	FAC Level	Energy (cm^{-1})		Uncert. (cm^{-1})[a]
Se	22+	$4s^24p^4$	$(4p+^2)_2$	1	0		
Se	22+	$4s4p^5$	$(4s+,(4p+^3)_{3/2})_2$	6	598 630		40
Se	22+	$4s4p^5$	$(4s+,(4p+^3)_{3/2})_1$	7	644 800		40
Se	22+	$4s^24p^34d$	$(4p+,4d-)_2$	8	728 230		60
Se	22+	$4s^24p^34d$	$(4p+,4d-)_3$	10	737 720		60
Se	22+	$4s^24p^34d$	$(4p+,4d-)_1$	11	752 630		60
Se	22+	$4s^24p^34d$	$(4p+,4d+)_2$	14	786 840		60
Se	22+	$4s^24p^34d$	$(4p+,4d+)_3$	16	820 220		60
Se	22+	$4s^24p^34d$	$((4p-,(4p+^2)_{2})_{3/2},4d+)_1$	28	949 650		110
Se	22+	$4s^24p^34d$	$((4p-,(4p+^2)_2)_{5/2},4d-)_2$	31	976 320		100
Se	22+	$4s^24p^34d$	$((4p-,(4p+^2)_{2})_{5/2},4d+)_3$	33	990 320		100
Se	22+	$4s^24p^34d$	$((4p-,(4p+^2)_2)_{5/2},4d-)_3$	36	1 018 600		100
As	23+	$4s^24p^3$	$(4p+)_{3/2}$	1	0		
As	23+	$4s4p^4$	$(4s+,(4p+^2)_2)_{5/2}$	6	573 520		30
As	23+	$4s4p^4$	$(4s+,(4p+^2)_2)_{3/2}$	7	640 620		40
As	23+	$4s^24p^24d$	$(4d-)_{3/2}$	10	758 920		60
As	23+	$4s^24p^24d$	$(4d+)_{5/2}$	12	798 540		60
As	23+	$4s^24p^24d$	$((4p-,4p+)_1,4d+)_{5/2}$	21	943 250		90
As	23+	$4s^24p^24d$	$((4p-,4p+)_1,4d+)_{3/2}$	22	952 840		90
As	23+	$4s^24p^24d$	$((4p-,4p+)_2,4d+)_{5/2}$	24	979 460		100
As	23+	$4s^24p^24d$	$((4p-,4p+)_2,4d-)_{3/2}$	26	987 170		100
As	23+	$4s^24p^24d$	$((4p-,4p+)_2,4d-)_{1/2}$	27	987 170		100
As	23+	$4s^24p^24d$	$((4p-,4p+)_1,4d+)_{3/2}$	28	1 018 960		100
As	23+	$4s^24p^24d$	$((4p-,4p+)_2,4d-)_{5/2}$	29	1 029 060		110
Ge	24+	$4s^24p^2$	$(4p-^2)_0$	1	0		
Ge	24+	$4s^24p^2$	$(4p-,4p+)_1$	2	142 076		FAC
Ge	24+	$4s^24p^2$	$(4p-,4p+)_2$	3	163 460	$+x$	
Ge	24+	$4s4p^3$	$(4s+,4p+)_1$	7	648 280		40
Ge	24+	$4s4p^3$	$((4s+,4p-)_0,(4p+^2)_2)_2$	8	709 880	$+x$	
Ge	24+	$4s4p^3$	$((4s+,4p-)_1,(4p+^2)_2)_2$	13	855 840	$+x$	
Ge	24+	$4s^24p4d$	$(4p-,4d-)_2$	14	899 590	$+x$	
Ge	24+	$4s^24p4d$	$(4p-,4d+)_3$	16	961 770	$+x$	
Ge	24+	$4s^24p4d$	$(4p-,4d-)_1$	17	983 410		100
Ge	24+	$4s^24p4d$	$(4p+,4d-)_3$	23	1 123 330	$+x$	
Ga	25+	$4s^24p$	$(4p-)_{1/2}$	1	0		
Ga	25+	$4s^24p$	$(4p+)_{3/2}$	2	172 050		70
Ga	25+	$4s4p^2$	$(4s+)_{1/2}$	3	434 550		20

Table 3. (Continued.)

Seq.	Stage	Config.	Level	FAC Level	Energy (cm^{-1})		Uncert. (cm^{-1})[a]
Ga	25+	$4s4p^2$	$((4s+,4p-)_1,4p+)_{5/2}$	5	592 150		90
Ga	25+	$4s4p^2$	$((4s+,4p-)_0,4p+)_{3/2}$	6	653 380		40
Ga	25+	$4s4p^2$	$((4s+,4p-)_0,4p+)_{1/2}$	7	682 930		50
Ga	25+	$4s4p^2$	$(4s+,(4p+^2)_2)_{5/2}$	8	753 230		80
Ga	25+	$4s4p^2$	$(4s+,(4p+^2)_2)_{3/2}$	10	861 450		60
Ga	25+	$4s4p^2$	$(4d-)_{3/2}$	11	970 410		70
Ga	25+	$4s^24d$	$(4d+)_{5/2}$	12	1 000 880		100
Ga	25+	4s4p4d	$((4s+,4p-)_1,4d+)_{5/2}$	7	1 450 250		90
Ga	25+	$4s^24f$	$(4f-)_{5/2}$	42	1 841 720		100
Zn	26+	$4s^2$	$(4s+^2)_0$	1	0		
Zn	26+	4s4p	$(4s+,4p-)_0$	2	402 494		FAC
Zn	26+	4s4p	$(4s+,4p-)_1$	3	429 160		20
Zn	26+	4s4p	$(4s+,4p+)_1$	5	675 710		50
Zn	26+	4s4d	$(4s+,4d-)_1$	11	1 360 840	$+x$	
Zn	26+	4s4d	$(4s+,4d+)_2$	14	1 471 280		60
Zn	26+	4s4f	$(4s+,4f+)_3$	30	2 287 450		90
Cu	27+	4s	$(4s+)_{1/2}$	1	0		
Cu	27+	4p	$(4p-)_{1/2}$	2	460 710		20
Cu	27+	4p	$(4p+)_{3/2}$	3	641 740		40
Cu	27+	4d	$(4d-)_{3/2}$	4	1 386 630		90
Cu	27+	4d	$(4d+)_{5/2}$	5	1 422 940		70
Cu	27+	4f	$(4f+)_{7/2}$	7	2 223 720		100
Si	42+	$3p^2$	$(3p-^2)_0$	1	0		
Si	42+	3p3d	$(3p-,3d-)_1$	10	2 184 000		500
Al	43+	$3s^23p$	$(3p-)_{1/2}$	1	0		
Al	43+	$3s^23p$	$(3p+)_{3/2}$	2	789 280	?	60
Al	43+	$3s3p^2$	$(3s+)_{1/2}$	3	866 390		80
Al	43+	$3s3p^2$	$((3s+,3p-)_1,3p+)_{3/2}$	6	1 729 600		300
Al	43+	$3s3p^2$	$((3s+,3p-)_1,3p+)_{1/2}$	7	1 794 500		300
Al	43+	$3s^23d$	$(3d-)_{3/2}$	8	2 100 400		400
Mg	44+	$3s^2$	$^1S_0$	1	0		
Mg	44+	3s3p	$(3s+,3p-)_1$	3	812 710		80
Mg	44+	3s3p	$(3s+,3p+)_1$	5	1 760 100		300
B	51+	$2s^22p$	2p−	1	0		
B	51+	$2s2p^2$	2s+	2	1 392 600		300
Be	52+	$2s^2$	$^1S_0$	1	0		
Be	52+	2s2p	$(2s+,2p-)_1$	3	1 081 460		140
Li	53+	2s	2s+	1	0		
Li	53+	2p	2p−	2	1 017 290		100

[a] FAC—energy calculated with the FAC code

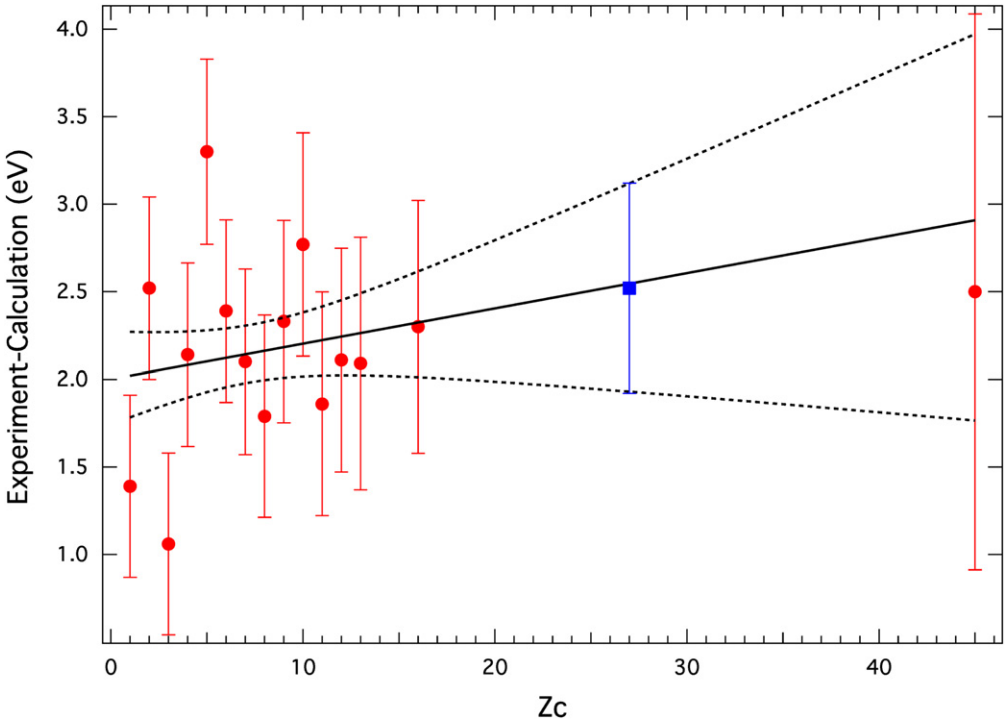

Figure 4. Differences of ionization energies from Dirac–Fock calculations [33] and measured values (values listed in the NIST Atomic Spectra Database) for Zn-like ions (filled circles). Z_c is the net charge of the core; $Z_c = Z - 29$. The plotted point for Ba (square) is the interpolated difference with estimated uncertainty.

Table 4. Calculated and observed ionization energies (eV) for Zn-like ions.

		Calc. binding energy [33]		Calc. Ion. Energy	Observed [32]		Obs.-Calc.
Z	Z_c	Zn-like	Cu-like		Ion. Energy	Uncert.	
30	1	48 799	48 791	8	9.394 1990	0.000 0022	1.39
31	2	52 815	52 797	18	20.515 14	0.000 12	2.52
32	3	57 010	56 977	33	34.0576	0.0012	1.06
33	4	61 381	61 333	48	50.14	0.06	2.14
34	5	65 930	65 865	65	68.30	0.10	3.30
35	6	70 657	70 572	85	87.390	0.025	2.39
36	7	75 562	75 455	107	109.1	0.1	2.10
37	8	80 646	80 515	131	132.79	0.25	1.79
38	9	85 909	85 753	156	158.33	0.25	2.33
39	10	91 351	91 168	183	185.77	0.37	2.77
40	11	96 974	96 761	213	214.86	0.37	1.86
41	12	102 778	102 534	244	246.11	0.37	2.11
42	13	108 764	108 487	277	279.09	0.50	2.09
45	16	127 821	127 434	387	389.3	0.5	2.30
56	27	212 199	211 264	935			
74	45	403 312	400 960	2352	2354.5	1.4	2.50

energies over the range $Z = 53$–59 ($Z_c = 24$–30). The result of this procedure for determining the ionization energy of Zn-like Ba is $(934.62 \pm 0.46)\,\text{eV} + (2.55 \pm 0.60)\,\text{eV} = (937.2 \pm 0.8)\,\text{eV}$.

Acknowledgements

This research was supported in part by the Office of Fusion Energy Sciences of the US Department of Energy. We thank A Kramida for helpful discussions concerning derivation of the ionization energy of Zn-like Ba.

References

[1] Morgan C A, Serpa F G, Takacs E, Meyer E S, Gillaspy J D, Sugar J, Roberts J R, Brown C M and Feldman U 1995 *Phys. Rev. Lett.* **74** 1716

[2] Crespo L-U Jr, Beiersdorfer P, Widmann K and Decaux V 1999 *Phys. Scr.* **T80** 448
[3] Crespo L-U Jr, Beiersdorfer P, Widmann K and Decaux V 2002 *Can. J. Phys.* **80** 1687
[4] Gillaspy J D, Osin D, Ralchenko Yu, Reader J and Blundell S A 2013 *Phys. Rev.* A **87** 062503
[5] Reader J and Luther G 1980 *Phys. Rev. Lett.* **45** 609
[6] Reader J and Luther G 1981 *Phys. Scr.* **24** 732
[7] Gillaspy J D 1997 *Phys. Scr.* **T71** 99
[8] Ralchenko Yu, Reader J, Pomeroy J M, Tan J N and Gillaspy J D 2007 *J. Phys. B: At. Mol. Opt. Phys.* **40** 3861
[9] Ralchenko Yu, Draganic I N, Osin D, Gillaspy J D and Reader J 2011 *Phys. Rev.* A **83** 032517
[10] Blagojević B *et al* 2005 *Rev. Sci. Instrum.* **76** 083102
[11] Holland G E, Boyer C N, Seely J F, Tan J N, Pomeroy J M and Gillaspy J D 2005 *Rev. Sci. Instrum.* **76** 073304
[12] Ralchenko Yu V and Maron Y 2001 *J. Quant. Spectrosc. Radiat. Transfer* **71** 609
[13] Osin D, Reader J, Gillaspy J D and Ralchenko Yu 2012 *J. Phys. B: At. Mol. Opt. Phys.* **45** 245001
[14] Ralchenko Yu and Gillaspy J D 2013 *Phys. Rev.* A **88** 012506
[15] Gu M F 2008 *Can. J. Phys.* **86** 675
[16] Ralchenko Yu, Draganić I N, Tan J N, Gillaspy J D, Pomeroy J M, Reader J, Feldman U and Holland G E 2008 *J. Phys.* B **41** 021003
[17] Otranto S, Olson R E and Beiersdorfer P 2006 *Phys. Rev.* A **73** 022723
[18] Acquista N and Reader J 1984 *J. Opt. Soc. Am.* B **1** 649
[19] Sugar J, Kaufman V, Baik D H, Kim Y-K and Rowan W L 1991 *J. Opt. Soc. Am.* B **8** 1795
[20] Seely J F, Brown C M and Feldman U 1989 *At. Data Nucl. Data Tables* **43** 145
[21] Kim Y K, Baik D H, Indelicato P and Desclaux J P 1991 *Phys. Rev.* A **44** 148
[22] Huang K N 1986 *At. Data Nucl. Data Tables* **34** 1
[23] Ekberg J O, Feldman U, Seely J F, Brown C M, MacGowan B J, Kania D R and Keane C J 1991 *Phys. Scr.* **43** 19
[24] Seely J F, Ekberg J O, Feldman U, Schwob J L, Suckewer S and Wouters A 1988 *J. Opt. Soc. Am.* B **5** 602
[25] Ivanova E P, Ivanov L N and Tsirekidze M A 1986 *At. Data Nucl. Data Tables* **35** 419
[26] Koc K 2005 *Nucl. Instrum. Methods Phys. Res.* B **235** 46
[27] Zhang H L and Sampson D H 1994 *At. Data Nucl. Data Tables* **56** 41
[28] Cheng K T, Chen M H and Johnson W R 2008 *Phys. Rev.* A **77** 052504
[29] Zhang H L and Sampson D H 1994 *At. Data Nucl. Data Tables* **56** 41
[30] Sapirstein J and Cheng K T 2011 *Phys. Rev.* A **83** 012504
[31] Kim Y K, Baik D H, Indelicato P and Desclaux J P 1991 *Phys. Rev.* A **44** 148
[32] Kramida A, Ralchenko Yu, Reader J and NIST ASD Team 2013 *NIST Atomic Spectra Database* version 5.1 (Gaithersburg, MD: National Institute of Standards and Technology) http://physics.nist.gov/asd
[33] Rodrigues G C, Indelicato P, Santos J P, Patte P and Parente F 2004 *At. Data Nucl. Data Tables* **86** 117
[34] Riyaz A, Tauheed A and Rahimullah K 2012 *J. Quant. Spectrosc. Radiat. Transfer* **113** 2072